Draft version September 26, 2022
Typeset using LaTeX **twocolumn** style in AASTeX631

The TESS Atlas: an open-source living catalog of TESS transit fits

Avi Vajpeyi[1,2] and Daniel Foreman-Mackey[3]

[1] *School of Physics and Astronomy, Monash University, Clayton VIC 3800, Australia*
[2] *OzGrav: The ARC Centre of Excellence for Gravitational Wave Discovery, Clayton VIC 3800, Australia*
[3] *Center for Computational Astrophysics, Flatiron Institute, New York, NY 10010, USA*

ABSTRACT

We present the TESS Atlas, a living catalog of candidate exoplanet parameter estimates, from two-minute cadence TESS data from 2018-2021. This catalog contains posterior estimates for 2,833 TESS Objects of Interest, including 157 multi-planet candidate systems and 81 candidates having data for a single transit. Our analysis utilises the No-U-Turns Markov chain Monte Carlo algorithm to sample the parameter space with a circular transit model implemented in exoplanet. We provide software, Jupyter notebooks and output files for all analyses so they can be easily reproduced, modified, and utilised in the future.

Keywords: methods: data analysis — methods: statistical — miscellaneous — catalogs — surveys

1. INTRODUCTION

In March 2022, NASA's exoplanet archive (Akeson et al. 2013) surpassed five thousand confirmed exoplanets, a milestone made possible by data from several observatories, including the Transiting Exoplanet Survey Satellite TESS (Ricker et al. 2015; Stassun et al. 2018, 2019; Guerrero et al. 2021). The confirmed exoplanets exhibit a wide range of masses, compositions, and radii. Some of these planets are also located within their planetary systems' habitable zone, e.g. TRAPPIST-1defg (Gillon et al. 2017; Wolf 2017; Agol et al. 2021), Teegarden's Star bc (Zechmeister et al. 2019), etc. Furthermore, the population of these exoplanets has fuelled research into planetary system architecture, planetary formation and evolution, and updated exoplanet occurrence rates (Winn & Fabrycky 2015; Sing et al. 2016; Emsenhuber et al. 2021; Zhu & Dong 2021). These analyses will be more informative with a bigger sample of exoplanets and more precise estimates of the planet's characteristics. This list of $\sim 5,000$ exoplanets may be dramatically increased once the $\sim 6,000$ candidates awaiting validation are processed, more than half of which are TESS Objects of Interest (TOIs).

Corresponding author: Daniel Foreman-Mackey
foreman.mackey@gmail.com

In this paper, we re-measure the planet parameters for all 2,833 of the TOIs with two-minute cadence observations from 2018 through 2021, assuming that the TOIs are from transiting planets. Our analysis provides realistic uncertainty estimates for the TOI's best-fit parameters and a uniform database of transiting exoplanet posterior estimates, which may be leveraged for future follow-up studies. Additionally, we build and publicly distribute Jupyter notebooks for the end-to-end analysis of each TOI, making the data products easy to reproduce and access. The notebooks are available on the catalog website (catalog.tess-atlas.cloud.edu.au).

The remainder of the paper is organised as follows. Section 2 outlines the procedures to analyse each TOI and generate the TESS Atlas. The catalog results are summarised in Section 3. The catalog data products, and software to reproduce the results available online as supplementary materials (catalog.tess-atlas.cloud.edu.au). Finally, we discuss caveats and provide concluding remarks in Section 4.

2. METHOD

2.1. *Target selection and data acquisition*

We obtain planetary parameters for 5,488TOIs with two-minute cadence data from the Exoplanet Follow-up Observing Program for TESS catalog (ExoFOP Guer-

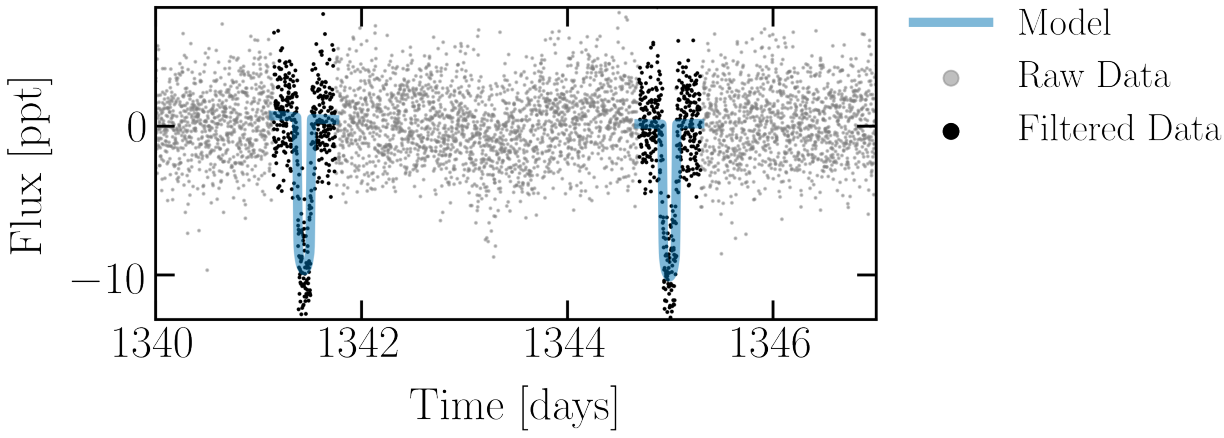

Figure 1. Light curve data for TOI 103 (from 1030-1450 BKJD): The raw light curve data for TOI 103 is plotted in gray, with the ExoFOP transit model plotted on top in blue. The black points are obtained by filtering the raw data using the ExoFOP transit parameter estimates as described in the text. Code to reproduce this plot is on GitHub.

rero et al. 2021).[1] This catalog reflects the best possible analysis when promoting transit search candidates into TOIs (Guerrero et al. 2021). Any TOIs lacking a period measurement, or a period equal to zero, are flagged as single-transit systems. We download the TOI light curves created by the TESS Science Processing Operations Center pipeline (Jenkins et al. 2016, 2021) using lightkurve (Lightkurve Collaboration et al. 2018).[2]

As a preliminary step, the light curve is filtered to remove low-frequency outliers. If the light curve dataset contains more than 100,000 data points, an additional filtering step is performed: data outside the anticipated ExoFOP transit times (with a buffer of two times the expected transit duration) are discarded. Figure 1 displays a plot of TOI 103's raw and filtered light curves, as well as ExoFOP's transit model Finally, parameter estimates for the radius and stellar density of each TOI's host star are retrieved from mast, if available.

2.2. *Transit Model*

The host star's limb darkening profile is approximated using Kipping (2013)'s quadratic limb darkening law (Claret 2000; Mandel & Agol 2002), parameterised in starry (Luger et al. 2019) by the baseline relative flux of the light curve f_0 and two quadratic limb-darkening parameters u_1, u_2. The stellar variability (from e.g. asteroseismic oscillation of the star) is modelled with a celerite (Foreman-Mackey et al. 2017) Gaussian Process (GP), with a stochastically driven damped harmonic oscillator kernel in linear combination with a jitter term J, to capture misspecified error bars and model misspecification. The GP requires three parameters: the quality factor $Q_{\rm GP}$, the undamped period of the oscillator $\rho_{\rm GP}$, and the standard deviation of the process $\sigma_{\rm GP}$. Exoplanet transits are modelled as circular (non-interacting) Keplerian orbits around their host star, using exoplanet (Foreman-Mackey et al. 2021). Circular orbits permit the use of computationally efficient, analytical orbital dynamics calculations. Additionally, circular orbits avoid degeneracies between eccentricity e, the argument of periastron ω, impact parameter b, and planet radius R_p. Furthermore, the eccentricity can also be computed in post-processing, as described by Dawson & Johnson (2012). Each of the n exoplanets in a system is parameterised by

1. *two reference transit times*, one near the beginning of the observations, $t_{\rm min}[n]$, and one near the end, $t_{\rm max}[n]$, both measured in TESS BJD,
2. *the number of periods*, $N_P[n]$, in the TESS observational baseline, between $t_{\rm min}$ and $t_{\rm max}$,
3. *the transit duration*, $\tau[n]$, measured in hours,
4. *the orbital impact parameter*, $b[n]$, constrained to be $|b| \leq 1$, and
5. *the radius ratio* $R_{\rm p}[n]/R_\star$, of the planet radius $R_{\rm p}[n]$ divided by the stellar radius $R_\star$.

[1] Data was downloaded from exofop.ipac.caltech.edu on July 28, 2022.

[2] All the TESS light curve data used in this paper can be found in MAST: https://doi.org/10.17909/t9-nmc8-f686.

The radius ratio is computed from the approximate transit depth, $\delta[n]$, measured in parts-per-thousand, using the small planet approximation

$$R_{\rm p}[n]/R_\star = \sqrt{\delta[n]}\,. \tag{1}$$

Additionally, the orbital period, $P[n]$, measured in days, can be calculated for each planet as

$$P[n] = (t_{\rm max}[n] - t_{\rm min}[n])/N_P[n]\,. \tag{2}$$

If a planet only transits once in observed data ($N_P[n] = 1$), we parameterize the model with $\{t_{\rm min}[n], P[n]\}$ instead of $\{t_{\rm min}[n], t_{\rm max}[n]\}$.

2.3. *Inference Framework*

Noise and stellar parameter priors: Uninformative priors are set for the stellar limb darkening (using the Kipping (2013) parameterisation), mean flux, and noise parameters. The quality factor $Q_{\rm GP}$ prior is fixed to a delta function at zero point three.

Transiting exoplanet priors: The transiting exoplanet parameter priors are centred around ExoFOP estimates. As transiting planet's phase and period are tightly constrained, we enforce a delta prior on the number of periods $N_P[n]$ between the two references times $t_{\rm min}[n]$ and $t_{\rm max}[n]$. The reference time priors are centred near the anticipated transit times and allowed a wide range of up to ten times the ExoFOP transit duration. If a planet only has a single-transit data recorded for a duration of time t, the prior on the second reference time $t_{\rm max}[n]$ is substituted with a prior on the planet's orbital period $P[n]$. As the orbital period for a single-transit planet is challenging to measure, a wide Pareto prior is placed on the period, with the minimum period $P_{\rm min}$ equal to

$$P_{\rm min}[n] = \max \begin{cases} t_{\rm min}[n] - \min(t) \\ \max(t) - t_{\rm min}[n] \end{cases}\,. \tag{3}$$

This prior provides more support for shorter periods. Importantly note that does not change the prior on $t_{\rm min}$ and $t_{\rm max}$ since the Jacobian is a constant $1/N_P$

We set a log-normal radius ratio prior, centred at the ExoFOP radius ratio measurement. This radius ratio prior provides more support for systems with smaller ratios. Finally, the impact parameter prior is uniform, conditioned on the radius ratio. A full list of the priors is presented in Table 1.

Posterior sampling: We initialise the posterior sampler at a high likelihood point, obtained by using exoplanet's non-linear optimisation framework. Following initial optimisation, the posterior distribution is sampled with PyMC3's Hamiltonian Monte Carlo (HMC) No U-Turn Sampler (Hoffman & Gelman 2011; Betancourt 2017; Salvatier et al. 2016). The sampler is run on two chains for 4,000 steps with a burn-in of 2,000 steps. We pass the chains to ArviZ and compute the rank normalised $\hat{R}$ diagnostic statistic Vehtari et al. (2019). Analyses with $\hat{R} > 1.01$ are considered failures due to convergence issues.

2.4. *Eccentricity post processing*

For successful analyses, we conduct a post-processing step to compute the orbital eccentricity, $e[n]$, and argument of periapsis, $\omega[n]$, for each transiting planet. We use our measurements of transit observables to compute the implied stellar density (under the assumption of circular orbits), $\rho_{\rm circ}[n]$. The expression for $\rho_{\rm circ}[n]$ is derived in Appendix A. Note that $\rho_{\rm circ}[n]$ is not the same as the actual stellar density, $\rho_\star$, and is unique for each planet in an n-planet system (see, for example, Dawson & Johnson 2012; Kipping et al. 2012). Following Dawson & Johnson (2012), we use $\rho_{\rm circ}[n]$ with a cataloged value of $\rho_\star$ (obtained from MAST) to generate weights. These are used to re-weight uniformly drawn $e[n]$ and $\omega[n]$ to get weighted posterior samples.

2.5. *Execution and catalog generation*

From data retrieval to post-processing, the analysis steps for a TOI are implemented in a 'template' Jupyter notebook.[3] After duplicating the template for each TOI, we insert the TOI number into each notebook and execute them in parallel with nbconvert. After execution, we use Jupyter-book, a sphinx-based package (Brandl 2021), to convert the notebooks into web pages. In addition to the analysis code, the pages display plots of the raw MAST and filtered light curves, HMC chain trace plots, posterior plots and phase-folded light curve plots of inferred orbits. The pages are deployed to the TESS Atlas website, alongside the Jupyter notebooks, raw data (the light curve data and ExoFOP estimates) and analysis outputs (the HMC chains and re-weighted posteriors). Finally, the median value and 1-σ bounds of all TOI posterior distributions are reported.

3. RESULTS

3.1. *Summary of the TESS Atlas catalog*

We analysed 2,833 two-minute cadence TOIs. From these, 3% analyses failed, most of which were TOIs with grazing transits ($b \gtrsim 0.9$). The successful analyses include 81 TOIs with a single transit in data and 357 TOIs in systems with multiple planets (in a total of 157

[3] github.com/dfm/tess-atlas/.../toi_template.py

Table 1. Priors table: Table of priors on the light curve transit model parameters. We use shorthand to represent distributions: $\mathcal{U}$ uniform (min, max), $\mathcal{N}$ normal (μ, σ), $\mathcal{P}$ar Pareto (α, min) and finally Inv-Γ Inverse Gamma (lower, upper). The prime superscript ($'$) indicates values from ExoFOP. Each planet in a n-planet system will have its unique planet priors. The t_i parameter is shorthand for both $t_{\rm min}$ and $t_{\rm max}$. The P prior is used only for planets with a single transit in data in place of $t_{\rm max}$. $P_{\rm min}$ is defined in the text. Finally, the prior on b is conditional on $R_{\rm p}/R_\star$ (refer to exoplanet documentation for details.)

Parameter	Distribution	Parameter	Distribution
Star		Planet[n]	
u_1, u_2	$\mathcal{U}(0,1)$	$R_{\rm p}/R_\star$	$\ln\mathcal{N}(R'_{\rm p}/R_\star, 1)$
f_0	$\mathcal{N}(0,10)$	b	$\mathcal{U}(0, R_{\rm p}/R_\star + 1)$
Noise		τ/days	$\ln\mathcal{N}(\ln\tau', 0.2) \in [4\,\text{min}, 10\tau']$
$\rho_{\rm GP}$	Inv-$\Gamma(0.5, 10)$	t_i/TBJD	$\mathcal{N}(t'_i, \tau') \in [t'_i \pm 10\tau']$
$\sigma_{\rm GP}, J$	Inv-$\Gamma(1,5)$	P/days	$\mathcal{P}\text{ar}(2/3, P_{\rm min})$
$Q_{\rm GP}$	0.3	N_P	N'_P

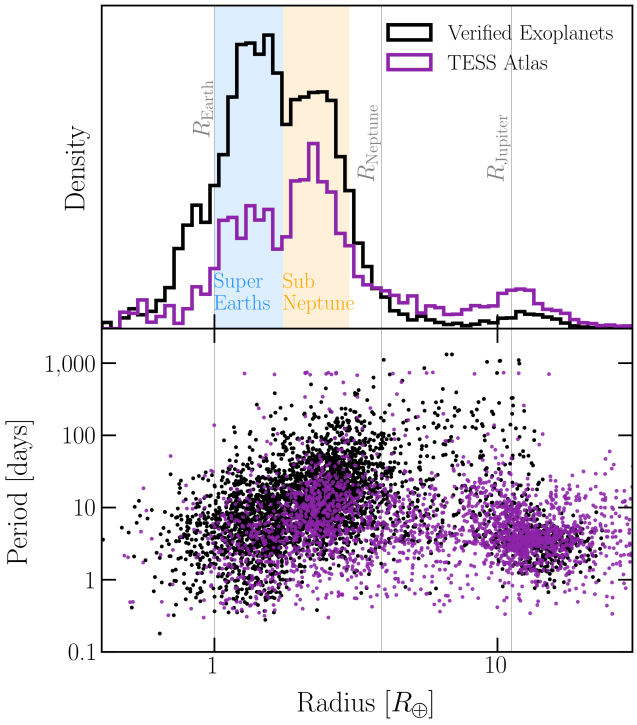

Figure 2. TOIs in period-radius space: (Top) Planet radii distribution. (Bottom) Planet period vs. radius scatter plot. The purple data are from the TESS Atlas fits, while the black data are from the population of verified transiting exoplanets, obtained from NASA's exoplanet archive. The code to reproduce this plot is on GitHub.

multi-planet systems). The catalog website displays the results for each TOI.

Figure 2 shows a plot of the TESS Atlas planetary periods and radii estimates (in purple). The top of the Figure displays the planetary radii distribution. We include the verified transiting exoplanet distribution from the NASA exoplanet archive (in black) to compare to the TESS Atlas catalog.[4] The Fulton et al. (2017) radius-gap is visible in the minor depletion of planets with radii between super-Earths and sub-Neptunes in both catalog radii distributions. Although the TESS Atlas has a lower super-Earth distribution, there is some agreement with the population of known exoplanets.

3.2. *Comparing with ExoFOP estimates*

To qualitatively assess the similarity between Atlas and ExoFOP inferred parameters, we superimpose ExoFOP measured values over the Atlas posterior and phase-folded light curve model plots. Figure 3.2 shows the phase-folded light curve plots for all five planets in TOI 174.[5] Each row displays the model predictions for one of the five planets. The datasets are folded on each planet's median period posterior value. The model's inferred orbits and 90% credible interval (CI) range are also folded and plotted in color on top of the black light curve data points. The model predictions using the ExoFOP orbit parameters are displayed with the dashed curves. The ExoFOP transit orbit parameters fall within the Atlas' 90% CI range, demonstrating visual consistency. This consistency between parameter estimates is highlighted in TOI 174.03's posterior plot in Figure 3.2. The ExoFOP $R_{\rm p}/R_\star, b, P, \tau$ values are plotted in red over the posteriors and lie within the 1-σ regions.

We estimate each TOI's $R_{\rm p}$ by multiplying the TESS Atlas median $R_{\rm p}/R_\star$ posterior value with the MAST stellar radii. To compare the TESS Atlas and ExoFOP catalog radii, we plot the two sets of radii against one another on the left side of Figure 3.2, while the right side displays the distribution of fractional change in planet radii between

[4] The NASA Exoplanet Science Institute's Planetary Systems Composite Table can be downloaded from: https://doi.org/10.26133/NEA13.

[5] The TESS Atlas catalog page for TOI 174 can be found here: catalog.tess-atlas.cloud.edu.au/.../toi_174.html.

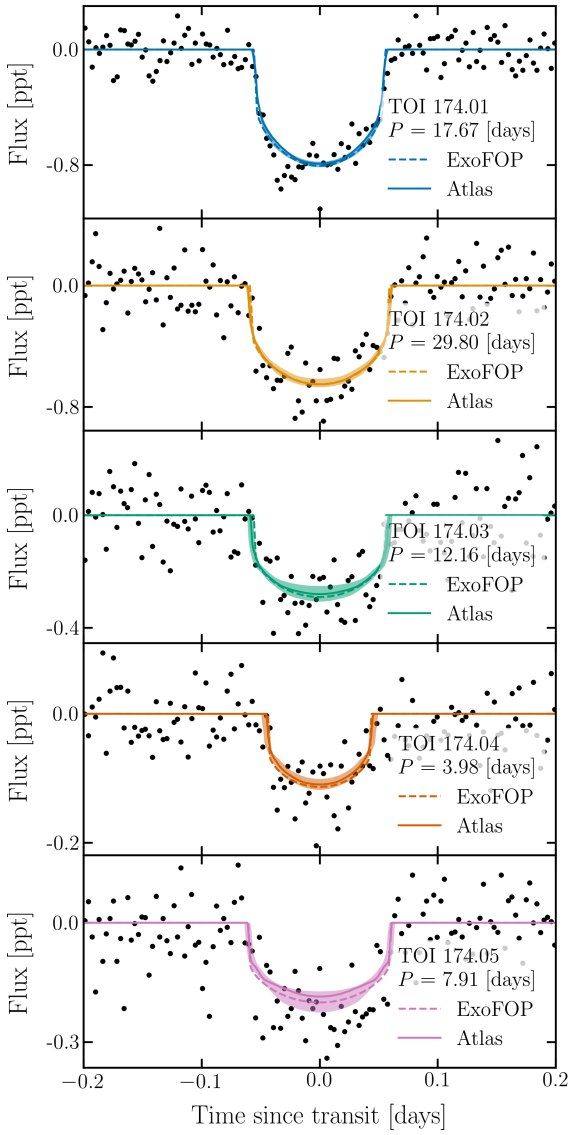

Figure 3. TOI 174 phase-folded light curve plots: De-trended light curves of the five TOI 174.01-.05 planets, folded each at each TOI's period posterior median value. The light curve data points (black) are binned to reduce visual clutter. The shaded regions display the inferred orbits' posterior constraints (the 90% CI region), while the solid curves show orbits from the posterior median value. Finally, the dashed curve depicts the model's orbits using ExoFOP orbital parameters.

the two catalogs. The black line plotted in both panels shows the 1:1 line between the two sets of posterior estimates. The TOIs with similar parameter estimates in both catalogs are found along this line. We find 80.3% of TOIs have TESS Atlas and ExoFOP radii estimates within 1-σ of each other. The median value of the fractional change plotted on the right side of Figure 3.2 is -7.2% with a standard deviation of 39.8%, indicating that TESS Atlas radii are systematically smaller than those in ExoFOP. Additionally, we find 3.7% of TOIs have radii that differ between the catalogs by more than 3σ. These discrepancies are attributable to variations between the TESS Atlas and ExoFOP analyses, including the data detrending method and the model parameterisation. Some of these TOIs may have $b \gtrsim 0.7$, in turn leading to inaccurate sampling (see e.g. Thompson et al. 2018; Gilbert 2022). Calculating the fractional difference between the ExoFOP and TESS Atlas period measurements, excluding systems with only a single transit, we see that the two catalogs are very consistent ($\sim 95\%$ of TOIs have a period fractional difference of less than 1%).

4. DISCUSSION AND CAVEATS

We present the first catalog of Bayesian posterior distributions for the two-minute cadence TOIs from 2018-2021. All posterior files and software for this work are publicly accessible. However, there are a few caveats users should be aware of when using the catalog. First, we model *all* TOIs with a circular transit model – even the TOIs that are assigned non-planet dispositions, such as eclipsing binaries. Additionally, the circular transit approximation will significantly overestimate the confidence of the impact parameter constraint (Gilbert 2022). For better measurements of the impact parameter,Gilbert (2022)'s umbrella sampling method with a grazing and non-grazing model should be used. Second, the orbits are modelled as non-interacting, even in the case of a multi-planet system. In multi-planet systems, gravitational interaction can perturb planet orbits leading to irregularly spaced transits. Third, Transit timing variations, correlated noise, and other systematics are ignored. Incorporating these can dramatically improve parameter measurements Coughlin et al. (2016); Thompson et al. (2018). Finally, No statistical tests other than the $\hat{R}$ check were performed to verify sampler convergence, so some of the catalog analysis may not be complete. However, even with these caveats, our transit analysis will be useful not only as a catalog for transiting exoplanet parameters, but each supplementary Jupyter notebook will be a useful starting point for future work on individual TOIs. We will periodically update the TESS Atlas catalog as longer-duration light curves are produced, and more TOIs are released to the public.

5. DATA AND SOFTWARE AVAILABILITY

We obtain the list of candidates from ExoFOP's publicly-accessible TOI page (Akeson et al. 2013), and use publicly-available light curve data (MAST: https://doi.org/10.17909/t9-nmc8-f686). We compare our results against the publicly-available Planetary Systems Composite Table created by the NASA Exoplanet

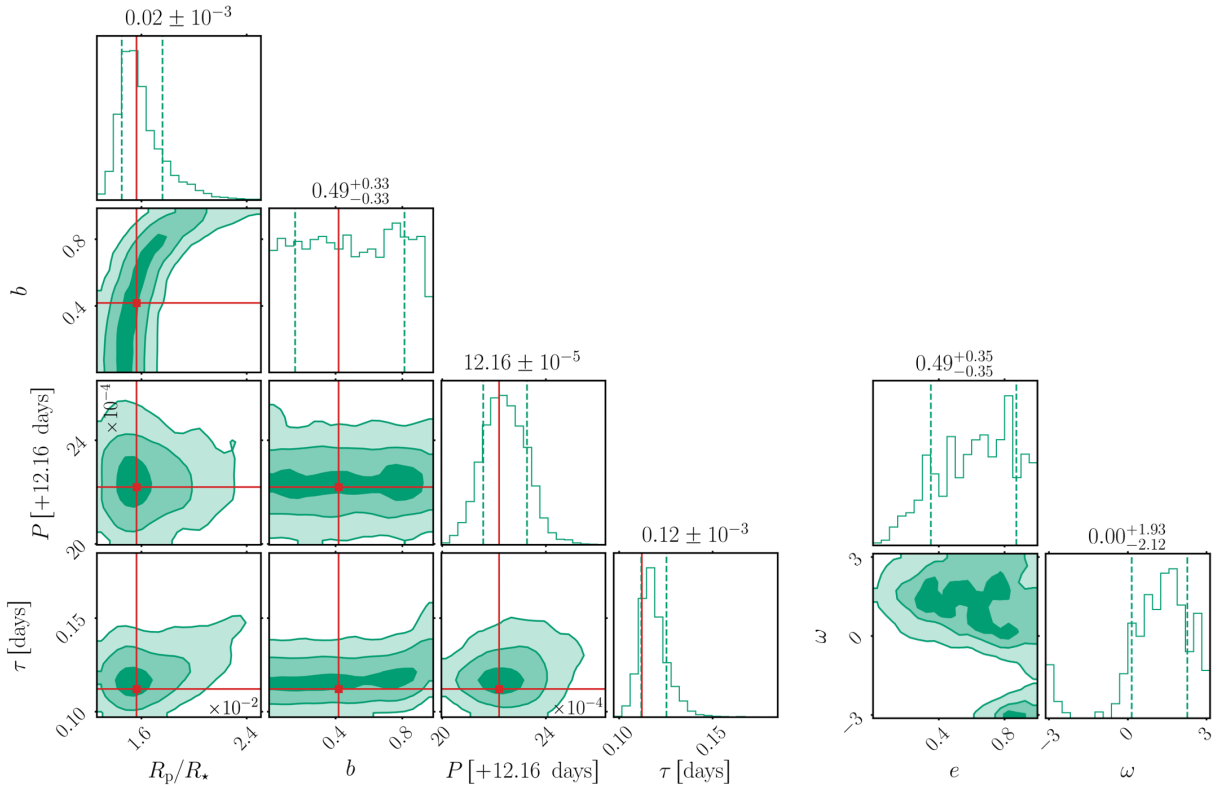

Figure 4. TOI 174.03 Posteriors: (Left) Radius ratio $R_p/R_\star$, impact parameter b, orbital period P and transit duration τ posteriors. (Right) Re-weighted posteriors for eccentricity e and the argument of periastron ω. The shaded regions depict the 1,2,3-σ contours. The 1D histograms dashed lines are the 90% credible intervals (CI). The numbers above the 1D histograms are the posterior median values with the 90% CI values as the uncertainties. The over-plotted red line indicates the ExoFOP transit parameters, except for e and ω. No values for e and ω are provided on TOI 174.03's ExoFOP page. Source code for this plot is provided in GitHub.

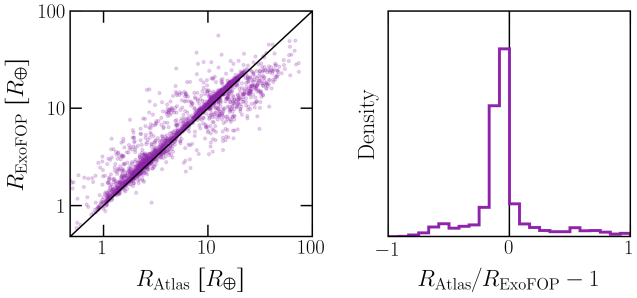

Figure 5. Comparison of ExoFOP and TESS Atlas radii measurements: (Left) A scatter plot of the ExoFOP TOI radii, R_{ExoFOP}, against the TESS Atlas TOI radii estimates, R_{Atlas}. The black line shows the one-to-one correspondence. (Right) Distribution of fractional change in planet radii between the two catalogs. Source code for this plot is provided in GitHub.

Science Institute (https://doi.org/10.26133/NEA13). We make our software (github.com/dfm/tess-atlas) and results (catalog.tess-atlas.cloud.edu.au) publicly accessible online. We additionally provide an application programming interface (API) to ease access to our data. The API is documented in the GitHub repository for this work.

ACKNOWLEDGMENTS

This work began during the 'online.tess.science' workshop in September 2020. The authors thank David Liptai, the OzStar and Nectar Openstack helpdesks, and the lightkurve developers for technical assistance. We also acknowledge discussions and historical contributions made by Nicholas Saunders, Joel Ong, Geert Barentsen and Jason Rowe.

We gratefully acknowledge the Swinburne Supercomputing OzSTAR Facility for computational resources. All analyses (including test and failed analyses) performed for this study used 127.6K core hours on OzSTAR. This would have amounted to a carbon footprint of $\sim$ 13t CO_2 (Australian Government - Department of the Environment and Energy 2021a,b). Thankfully, as OzSTAR is powered by wind energy from Iberdrola Australia; the electricity for computations produces negligible carbon waste.

The catalog is hosted on the Nectar Research Cloud. The Nectar Research Cloud is a collaborative Australian

research platform supported by the NCRIS-funded Australian Research Data Commons (ARDC).

This work has used the TIC through the TESS Science Office's target selection working group (architects K. Stassun, J. Pepper, N. De Lee, M. Paegert, R. Oelkers). This research has used the NASA Exoplanet Archive, which is operated by the California Institute of Technology, under contract with the National Aeronautics and Space Administration under the Exoplanet Exploration Program. Some of the data presented in this paper were obtained from the Mikulski Archive for Space Telescopes (MAST) at the Space Telescope Science Institute. The specific observations analyzed can be accessed via https://doi.org/10.17909/t9-nmc8-f686. STScI is operated by the Association of Universities for Research in Astronomy, Inc., under NASA contract NAS5–26555. Support to MAST for these data is provided by the NASA Office of Space Science via grant NAG5–7584 and other grants and contracts.

A.V. is supported by the Australian Research Council (ARC) Centre of Excellence CE170100004.

Facilities: TESS, MAST, Exoplanet Archive.

Software: Python (Oliphant 2007; Millman & Aivazis 2011), astropy (Price-Whelan et al. 2018), ArviZ (Kumar et al. 2019), exoplanet (Foreman-Mackey et al. 2021), lightkurve (Lightkurve Collaboration et al. 2018), starry (Luger et al. 2019), celerite (Foreman-Mackey et al. 2017), PyMC3 (Salvatier et al. 2016), numpy (Harris et al. 2020), scipy (Virtanen et al. 2020), pandas (Reback et al. 2020), matplotlib (Hunter 2007), corner (Foreman-Mackey 2016), sphinx (Brandl 2021), Jupyter (Kluyver et al. 2016), Jupyter-book (Executable Books Community 2020).

REFERENCES

Agol, E., Dorn, C., Grimm, S. L., et al. 2021, PSJ, 2, 1, doi: 10.3847/PSJ/abd022

Akeson, R. L., Chen, X., Ciardi, D., et al. 2013, PASP, 125, 989, doi: 10.1086/672273

Australian Government - Department of the Environment and Energy. 2021a, National Greenhouse Gas Inventory: Quarterly updates, Department of the Environment and Energy. https://www.industry.gov.au/data-and-publications/national-greenhouse-gas-inventory-quarterly-updates

—. 2021b, Carbon calculator, Department of the Environment and Energy. https://www.powershop.com.au/carbon-calculator/

Betancourt, M. 2017, arXiv e-prints, arXiv:1701.02434. https://arxiv.org/abs/1701.02434

Brandl, G. 2021, URL http://sphinx-doc. org/sphinx. pdf

Claret, A. 2000, A&A, 363, 1081

Coughlin, J. L., Mullally, F., Thompson, S. E., et al. 2016, ApJS, 224, 12, doi: 10.3847/0067-0049/224/1/12

Dawson, R. I., & Johnson, J. A. 2012, ApJ, 756, 122, doi: 10.1088/0004-637X/756/2/122

Emsenhuber, A., Mordasini, C., Burn, R., et al. 2021, A&A, 656, A70, doi: 10.1051/0004-6361/202038863

Executable Books Community. 2020, Jupyter Book, v0.10, Zenodo, doi: 10.5281/zenodo.4539666

Foreman-Mackey, D. 2016, The Journal of Open Source Software, 1, 24, doi: 10.21105/joss.00024

Foreman-Mackey, D., Agol, E., Ambikasaran, S., & Angus, R. 2017, celerite: Scalable 1D Gaussian Processes in C++, Python, and Julia, Astrophysics Source Code Library, record ascl:1709.008. http://ascl.net/1709.008

Foreman-Mackey, D., Luger, R., Agol, E., et al. 2021, The Journal of Open Source Software, 6, 3285, doi: 10.21105/joss.03285

Fulton, B. J., Petigura, E. A., Howard, A. W., et al. 2017, AJ, 154, 109, doi: 10.3847/1538-3881/aa80eb

Gilbert, G. J. 2022, AJ, 163, 111, doi: 10.3847/1538-3881/ac45f4

Gillon, M., Triaud, A. H. M. J., Demory, B.-O., et al. 2017, Nature, 542, 456, doi: 10.1038/nature21360

Guerrero, N. M., Seager, S., Huang, C. X., et al. 2021, ApJS, 254, 39, doi: 10.3847/1538-4365/abefe1

Harris, C. R., Millman, K. J., van der Walt, S. J., et al. 2020, Nature, 585, 357, doi: 10.1038/s41586-020-2649-2

Hoffman, M. D., & Gelman, A. 2011, arXiv e-prints, arXiv:1111.4246. https://arxiv.org/abs/1111.4246

Hunter, J. D. 2007, Computing in science & engineering, 9, 90

Jenkins, J. M., Twicken, J. D., McCauliff, S., et al. 2016, in Society of Photo-Optical Instrumentation Engineers (SPIE) Conference Series, Vol. 9913, Software and Cyberinfrastructure for Astronomy IV, ed. G. Chiozzi & J. C. Guzman, 99133E, doi: 10.1117/12.2233418

Jenkins, J. M., Twicken, J. D., Caldwell, D. A., et al. 2021, in Posters from the TESS Science Conference II (TSC2), 183, doi: 10.5281/zenodo.5136731

Kipping, D. M. 2013, MNRAS, 435, 2152, doi: 10.1093/mnras/stt1435

Kipping, D. M., Dunn, W. R., Jasinski, J. M., & Manthri, V. P. 2012, MNRAS, 421, 1166, doi: 10.1111/j.1365-2966.2011.20376.x

Kluyver, T., Ragan-Kelley, B., Pérez, F., et al. 2016, in Positioning and Power in Academic Publishing: Players, Agents and Agendas, ed. F. Loizides & B. Schmidt, IOS Press, 87 – 90

Kumar, R., Carroll, C., Hartikainen, A., & Martin, O. 2019, Journal of Open Source Software, 4, 1143, doi: 10.21105/joss.01143

Lightkurve Collaboration, Cardoso, J. V. d. M., Hedges, C., et al. 2018, Lightkurve: Kepler and TESS time series analysis in Python, Astrophysics Source Code Library, record ascl:1812.013. http://ascl.net/1812.013

Luger, R., Agol, E., Foreman-Mackey, D., et al. 2019, AJ, 157, 64, doi: 10.3847/1538-3881/aae8e5

Mandel, K., & Agol, E. 2002, ApJL, 580, L171, doi: 10.1086/345520

Millman, K. J., & Aivazis, M. 2011, Computing in Science Engineering, 13, 9, doi: 10.1109/MCSE.2011.36

Oliphant, T. E. 2007, Computing in Science Engineering, 9, 10, doi: 10.1109/MCSE.2007.58

Price-Whelan, A. M., Sipőcz, B., Günther, H., et al. 2018, The Astronomical Journal, 156, 123

Reback, J., McKinney, W., jbrockmendel, et al. 2020, pandas-dev/pandas: Pandas 1.0.2, v1.0.2, Zenodo, doi: 10.5281/zenodo.3708035

Ricker, G. R., Winn, J. N., Vanderspek, R., et al. 2015, Journal of Astronomical Telescopes, Instruments, and Systems, 1, 014003, doi: 10.1117/1.JATIS.1.1.014003

Salvatier, J., Wiecki, T. V., & Fonnesbeck, C. 2016, PyMC3: Python probabilistic programming framework, Astrophysics Source Code Library, record ascl:1610.016. http://ascl.net/1610.016

Sing, D. K., Fortney, J. J., Nikolov, N., et al. 2016, Nature, 529, 59, doi: 10.1038/nature16068

Stassun, K. G., Oelkers, R. J., Pepper, J., et al. 2018, AJ, 156, 102, doi: 10.3847/1538-3881/aad050

Stassun, K. G., Oelkers, R. J., Paegert, M., et al. 2019, AJ, 158, 138, doi: 10.3847/1538-3881/ab3467

Thompson, S. E., Coughlin, J. L., Hoffman, K., et al. 2018, ApJS, 235, 38, doi: 10.3847/1538-4365/aab4f9

Vehtari, A., Gelman, A., Simpson, D., Carpenter, B., & Bürkner, P.-C. 2019, arXiv e-prints, arXiv:1903.08008. https://arxiv.org/abs/1903.08008

Virtanen, P., Gommers, R., Oliphant, T. E., et al. 2020, Nature Methods, 17, 261, doi: 10.1038/s41592-019-0686-2

Winn, J. N. 2010, arXiv e-prints, arXiv:1001.2010. https://arxiv.org/abs/1001.2010

Winn, J. N., & Fabrycky, D. C. 2015, ARA&A, 53, 409, doi: 10.1146/annurev-astro-082214-122246

Wolf, E. T. 2017, ApJL, 839, L1, doi: 10.3847/2041-8213/aa693a

Zechmeister, M., Dreizler, S., Ribas, I., et al. 2019, A&A, 627, A49, doi: 10.1051/0004-6361/201935460

Zhu, W., & Dong, S. 2021, ARA&A, 59, 291, doi: 10.1146/annurev-astro-112420-020055

APPENDIX

A. COMPUTING THE IMPLIED STELLAR DENSITY

For a circular orbit, the transit duration is (Winn 2010)

$$\tau = \frac{P}{\pi} \sin^{-1}\left(\frac{\sqrt{(1+(R_p/R_\star)^2) - b^2}}{a \sin i}\right) \quad . \tag{A1}$$

where a is the semi-major axis in units of $R_\star$. Rearranging Eq A1 in terms of a, we find that

$$a^2 \sin^2 i \sin^2\left(\frac{\pi\,\tau}{P}\right) = (1+(R_p/R_\star)^2) - b^2 \quad . \tag{A2}$$

Since $\cos^2 i = b^2/a^2$, Eq A2 can be simplified

$$a^2 = \frac{(1+R_p/R_\star)^2 - b^2 \cos^2\phi}{\sin^2\phi} \tag{A3}$$

for $\phi = \pi\,\tau/P$.

Finally, under the assumption of a circular orbit, we can compute the implied stellar density $\rho_{\rm circ}$ with the period and semi-major axis

$$\rho_{\rm circ} = \frac{3\,\pi\,a^3}{G\,P^2} \quad . \tag{A4}$$